DISSOCIATION PHENOMENA IN ELECTRON-BEAM SUSTAINED CARBON DIOXIDE LASERS

Michael R. Harris and David V. Willetts
Royal Signals and Radar Establishment
Great Malvern, Worcestershire WR14 3PS, UK

INTRODUCTION

A number of applications are emerging requiring efficient, long pulse, long-life sealed CO_2 lasers. Examples include the proposed NASA and ESA wind lidars. Electron-beam sustained discharge devices are strong contenders. Unlike self-sustained discharges e-beam sustenance readily provides efficient performance from large volume discharges and offers pulse lengths well in excess of the microsecond or so generally associated with self-sustained devices.

In the case of the e-beam sustained laser, since the plasma is externally maintained and operated at electric field strengths less than that associated with the glow to arc transition, the discharges can be run even in the presence of strongly attacking species such as O_2. Build up of large levels of attacking contaminants is nevertheless undesirable as their presence reduces the current drawn by the plasma and thus the pumping rate to the upper laser level. The impedance rise leads to a mismatch to the pulse forming network with a consequent loss of control over energy deposition, operating E/N, and gain.

Clearly CO_2 dissociation rates, the influence of dissociation products on the discharge and gain, and tolerance of the discharge to these products need to be determined. This information can then be used to assess co-oxidation catalyst requirements for sealed operation.

CARBON DIOXIDE DISSOCIATION

Experimental Apparatus

The equipment used for the oxygen tolerance determination is shown schematically in Figure 1. The electron gun was a cold cathode plasma device run at a pressure of a few tens of microns of helium which was continuously bled in and pumped out by a Roots blower/backing pump combination. This type of gun has been described elsewhere (ref 1); briefly an auxiliary glow discharge is maintained in the drift region and provides ions for acceleration by the pulsed electric field. Secondary electrons emitted from the cathode are accelerated through a capacitative voltage dividing structure to provide an internal gun current of about an amp. The 150kV voltage pulse is delivered by a 6 mesh PFN of total capacitance 0.3μF and total inductance 918μH, switched by a thyratron through the primary of a 10:1 turns ratio pulse transformer. Gun current and voltage could be monitored by inductive loop and resistive division probes and recorded on a storage oscilloscope. The area of the foil separating the main discharge chamber and the gun was 30 x 2cm^2.

The main discharge chamber was constructed almost entirely of Monel, except that Viton O-rings were used for the demountable seals, the foil separating the gun from the main discharge was 25μm aluminium, and insulating lead throughs were made of PTFE. The removable discharge limiters were constructed of alumina. For the majority of the experiments the Monel grid protecting the foil was operated as the anode so that the cathode material could readily be changed. The

should be noted that Judd's value of T_e of 0.37eV is hardly more than half of Lowke Phelps and Irwin's value of 0.7eV. For all the subsequent calculations we quote both values with the parenthetic note (J) for the 0.37eV and (LPI) for the 0.70eV case. Using values of ϵ_j and Q_{oj} applicable to dissocation (6.2eV and 3.5×10^{-17} cm^2; reference 5) and dissociative attachment (3.9eV and 1.5×10^{-19} cm^2; reference 6), we found similar rates for both processes, but these were in excess of three orders of magnitude lower than experimental findings. This suggests that dissociation is not a bulk process but may be confined to the (cathode) sheath region. This lead us to repeat the dissociation measurement with the gap reduced from 2cm to 1cm and in support of this conjecture it was found that the dissociation rate was unaltered within experimental error. Further measuremets were carried out at halved E/N, and also with the cathode changed from Monel to Dural (a hardened Al alloy), and to 60/40 brass. Also explored was the effect of altering the electrode polarity so that dissociation takes place on the grid rather than on the smoothly profiled electrode. These changes did not significantly alter the dissocation rate either; addition of alumina discharge limiters increased the dissociation rate by about 10%, which we suspect to be due to field distortions caused by the presence of the thick high permittivity limiters. All this evidence is shown in Figures 7 and 8 and points toward dissociation in the sheath region; we have made initial attempts to estimate the magnitude of this process.

It is probably fair to say that the detail of the cathode fall mechanism is not well understood. J J Thomson (ref 7) derived the form of potential fall in a gap which is externally sustained and in which the electron loss process is by recombination. This theory is readily altered to encompass the attachment loss mechanism operative in our device (see below) but unfortunately the assumption that the loss mechanism can be neglected in the sheath leads to preposterous values of cathode fall Φ and sheath thickness L. A much better model has been provided by N G Basov (ref 8) who has adapted the von Engel and Steenbeck treatment of self-sustained discharges for the nonself-sustained case. The assumptions are

1. Electron emission from the cathode occurs solely by positive ion bombardment, so that

$$j_e = \gamma j_+$$

2. The field varies linearly in the sheath,

$$E(X) = E_o(1-X/L)$$

where X is the distance from the cathode.

Hence from Poisson's equation, ρ is a constant and since

$$\frac{n_+}{n_e} = \frac{j_+ v_e}{j_e v_+} = \gamma^{-1} \frac{v_e}{v_+} >> 1,$$

$$\rho = \rho_+ = \frac{1}{4\pi} \left[\frac{E_o}{L}\right]$$

3. The positive ion velocity v_+ is constant in the sheath, implying that j_+ is constant and

$$v_+ = \frac{4\pi j_+}{(E_o/L)} = \frac{4\pi j_{tot}}{(E_o/L)} \quad \text{since } \gamma << 1.$$

changing dissociation rate as N_e changes as a consequence of oxygen buildup, ie significant curvature should be expected in Figures 5, 7 and 8. It may well be that dissociation is taking place in the negative glow region rather than the cathode fall. It is important to note that the lack of volume scaling indicates that the result should be applicable to any e-beam sustained laser device.

Dissociation by Primary Beam Alone

The results quoted above obviously indicate dissociation by both main discharge and primary electron beam. The latter has a very high energy of about one hundred keV at which dissociative cross sections are very small. Thus bulk dissociation due to primaries is not expected to be an important process. Exactly the same method was used to assess the effect of the primary beam alone as already described, except that the collector electrode was 'earthed' through a 50ohm resistive current probe. Figure 9 illustrates the findings with a linear buildup of oxygen with number of pulses at a rate dependent on current within the pulse. Figure 10 shows that the dependence on current is linear and so the dissociation scales linearly with charge passed. Much more surprising is the independence on the volume exposed to primaries, very similar to the observations on the main discharge. It would thus appear that a surface mediated effect is being observed which was quite unexpected. A further experiment was performed of varying widely the carbon dioxide partial pressure in the gas mixture, starting with a system cleaned by evacuation and repetitive pulsing of the gun and gradually increasing pCO_2. Figure 11 records the results which are absorption isothermal in form, suggestive of a true surface dissociation. However, the rate is amazingly high, at 15mmole/coulomb for the 3/2/1 mixture. This corresponds to 3000 CO_2 molecules being broken up for each primary electron passed which corresponds to a few monolayers/pulse and an overall efficiency of about 20% of total primary beam energy going into dissociation. The primary process appears to be contributing 10-15% of the total cracking observed in the main discharge.

A number of possible mechanisms have been investigated theoretically to account for the large dissociation by the primary beam. These include:

1. Cracking by the fast initial secondaries which have an energy of 30-40eV and thermalise in about 1ns. A bulk effect of 2.4 molecules/electron for a one centimetre gap.

2. Dissociation by thermalised secondaries. At equilibrium, rate of loss by dissociative attachment equals rate of ionisation, so the ionisation and dissociation rates become equal. This is also a bulk process with 13 molecules dissociated/electron crossing a one centimetre gap.

3. Effect of secondary electrons emitted from the electrode surface by the impact of the primary beam or of the fast nonthermalised bulk secondary electrons near the surface. The latter are found to predominate, but the emitted secondaries peak at only 2-3eV energy so the dissociation they give rise to is very small, about 0.1 molecule/primary electron. Although this is a surface mediated effect which is expected to be volume independent, it is of insignificant magnitude.

4. Thermal effects. Thermodynamic data (ref 9) gives

$$\Delta G^{\circ} = -135100 + 41.5T$$

for the process

$$2CO_2 \rightarrow 2CO + O_2$$

Thus $\ln Kp \equiv 6.82 \times 10^4/T - 20.96$

where

$$\frac{I_s}{I_p} = \frac{J_s}{J_p} = \frac{n_e e \bar{v}}{S_o e} \sum_i \sigma_i N_i$$

$$\therefore \frac{I_s}{I_p} = \frac{\bar{\nu}}{\beta} \sum_i \sigma_i N_i \qquad (2)$$

Taking σ_{N2} to be 1.5 x $10^{-18}cm^2$ and σ_{He} = 0.3 x $10^{-18}cm^2$,

$$\sum_i \sigma_i N_i$$

is $17.4cm^{-1}$ for a 1 atm 3/2/1 mixture. $\bar{\nu}$ is known to be 4.4 x 10^6 cm sec^{-1} for this mixture and E/N (refs 3, 4). β was evaluated from an overlap integral of the form of equation (1) with the values of Q_{oi} and ϵ_i enjoyed by dissociative attachment to carbon dioxide; a value of 7.7 x 10^3 (J) and 9.4 x 10^5 (LP&I) sec^{-1} were found. Thus the predicted value of 3660 (J) is in remarkable agreement, considering the approximations, with the slope of Figure 12 namely 3750. The LPI prediction is for I_s/I_p = 30. Inclusion of alumina discharge limiters alters the ratio to 2700, which we presume to result from field distortions arising from inclusion of a substantial thickness of high dielectric constant material.

Composition Dependence of Secondary to Primary Current Ratio

The ratio of secondary to primary currents was measured for a variety of gas compositions. Figure 12 compares the results of experiments on 3:2:1 and 13:2:1 gas mixtures, these results and a number of others are listed in Table 1. The results can be understood from formula (2) above.

The drift velocity $\bar{\nu}$ varies weakly with composition, but the attachment coefficient β varies strongly and like the ionisation cross section, may be written as

$$\beta = \sum_i \beta_i N_i$$

Since the attachment coefficients of nitrogen and helium are much less than that of CO_2, and σ_{He} is very small

$$\frac{I_s}{I_p} \simeq \frac{\bar{\nu}\sigma_{N_2}}{\beta_{CO_2}} \left[\frac{y}{z} + \frac{\sigma_{CO_2}}{\sigma_{N_2}}\right]$$

for a x:y:z $He:N_2:CO_2$ gas mixture. It is immediately apparent that M should be constant for a fixed ratio of N_2 to CO_2, independent of the helium content of the mixture. This prediction is well borne out for y = 2, z = 1, and x = 13, 3 and 0. Examining the pure CO_2 ratio, and taking $\beta(CO_2)\bar{\nu}$ to be about $10^{-21}cm^2$ for CO_2 at 4kV/cm atm, we find $\sigma(CO_2)$ to be roughly 3 x $10^{-17}cm^2$, considerably less than $\sigma(N_2)$. Thus to a good approximation,

where the k_i's are the electron and gas temperature dependent three body coefficients for each of the neutral species i present in the gas mixture, which have been measured by Chanin et al (ref 11). The values at T_e = 0.36eV are 2 x 10^{-32}, 2 x 10^{-30} and ~ $10^{-33}cm^6sec^{-1}$ for N_2, O_2 and He respectively falling to $\leqslant$ 1 x 10^{-32}, 1 x 10^{-30} and $\approx 10^{-34}$ at T_e = 0.7eV. The values for H_2O and CO_2 are tabulated at a mean electron energy of 0.03eV only, where they are 2 x 10^{-29} and 3 x $10^{-30}cm^6sec^{-1}$ respectively. Thus

$$\frac{\partial Z}{\partial N_{O_2}} = \frac{V_s \sum_i k_i N_i}{I_p \bar{\nu} \sum_i \sigma_i N_i}$$

The k_i and σ_i for i = He may be neglected; if these coefficients are also neglected for CO_2, oxygen and water, we find

$$\frac{\partial Z}{\partial N_{O_2}} = \frac{V_s k_{N_2}}{I_p \bar{\nu} \sigma_{N_2}} = 2.7 \times 10^{-16}\ \Omega\ cm^3\ (0.36eV)$$

$$\leqslant 1.3 \times 10^{-16}\ \Omega\ cm^3\ (0.7eV)$$

in good agreement with the experimental determination. It is difficult to justify the neglect of the k_i's for O_2, H_2O and CO_2 except for the fact that the latter pair are ill-determined; at face value the oxygen k_i should introduce significant curvature into the graph of Figure 13. The influence of discharge-produced oxygen is shown in Figure 14. Here we have plotted the discharge resistivity rather than impedance with allows ready scaling to other discharge dimensions or for the presence of discharge limiters. It is apparent that the dissociation products influence the discharge in the same way as deliberately added oxygen, the impedance doubling at an oxygen concentration of about one per cent. This fact is consistent with the observation that carbon monoxide has no influence on the discharge impedance.

GAIN MEASUREMENTS

Methodology

The optical arrangement used to measure the gain in the amplifier is shown in Figure 15; it relies on the usual method of probing with a low power cw laser. The output from this cw laser was transmitted by variable attenuators of CaF_2 and then double passed through the gain medium. The probe beam was focussed onto the surface of a room-temperature CMT photoconductive detector whose output voltage was amplified and displayed by a storage oscilloscope. Although the oscilloscope was restricted to a maximum bandwidth of 1MHz it was confirmed that this response was more than adequate for the long pulse observations of interest. A removable mirror allowed the operating transition of the cw laser to be examined using a wavelength monitor; the probe laser was set on the 10P(20) line for all measurements by adjustment of its cavity length, by control of the voltage on the piezoelectric transducer to which one vacity mirror was attached. Two periscopes, omitted from the diagram for clarity, changed the height of the probe beam out of the plane of the diagram in passing through the lead X-ray shield around the gain cell. The polarisation of the cw probe was roughly parallel with the main discharge electric field.

Thus Q_r, the charge remaining on the PFN at the end of the pulse is

$$Q_r = Q_o - Q_{lost} = \left[\frac{M-1}{M+1}\right] Q_o$$

and so V_r, the voltage remaining on the device at the end of the pulse is

$$V_r = \frac{Q_r}{C_o} = \frac{Q_o}{C_o}\left[\frac{M-1}{M+1}\right] = V_o\left[\frac{M-1}{M+1}\right]$$

Similarly, the energy E deposited by the discharge is

$$E = IV\tau = \frac{2C_o MV_o^2}{(1+M)^2}$$

which at match equals $\frac{1}{2}C_oV_o^2$; thus the fraction F of energy deposited compared with the matched case is given by

$$F = \frac{4M}{(1+M)^2}$$

In Figure 20 the voltage multiplication factor 2M/1+M, fractional voltage remaining V_r/V_o = M−1/M+1, and F are plotted vs the impedance multiplication factor M, which is a function of oxygen present in the discharge. Clearly for M = 1.5 which corresponds to ½% oxygen, V/V_m = 1.2, V_r/V_o = 0.20 and F = 0.96. This means that the operating E/N would exceed the design value for 0% oxygen by 20%, a residual E/N of 40% $(E/N)_{design}$ would remain after the pulse, and 96% of design energy would be delivered to the plasma. Although we have yet to elaborate on the residual voltage, these figures suggest that even without any measures being taken to counteract the oxygen produced, a level of ½% should be tolerable.

It is instructive to compare the energy deposited in Figure 20 with the small signal gain of Figure 18. For a matched design E/P of 4kV/cm atm, at 170 A secondary current the gain equals 1.92% cm^{-1}; for M = 1.86, we find an actual E/P of 5.2kV/cm atm, F = 0.91, and I = 119A so that the gain becomes 2.35% cm^{-1}. As the discharge moves out of match the gain changes along the broken line in Figure 18. Thus as the energy deposition falls the small signal gain g_o rises. This happens because the output energy g_oE_sL depends also on the saturation parameter E_s which we have not investigated.

Discharge Stability

The design E/N is well below the region of the attachment instability, so an arc will develop in the main discharge only if the instantaneous value of E/N gets too high. The previous section deals with the effect of impedance matching on the field E during and after the conduction phase; thus information is also required on the gas density N. The latter changes during the period of energy deposition due to gas heating and consequent expansion, which lowers N and raises E/N. Clearly such a rapid expansion must be adiabatic, and with the assumption of reversibility has been treated by Baranov and Breev (ref 13) who find for the ratio of densities before and after expansion

conduction and could lead to breakdown, depending on the PFN risetime. Such mismatches should not be encountered since they require inordinately high PFN charging voltages and dissociation products increase the value of M. For these reasons we have not encountered post conduction phase arcs.

Discharge stability is thus governed by the design E/N and energy loading, but especially by matching criteria for the PFN and discharge impedance.

SUMMARY

1. The oxygen concentration was found to rise linearly with charge passed, at a rate of 30 μmole/Coulomb. This dissociation rate was independent of volume, implying effects in the cathode fall or negative glow regions. The result should therefore be applicable to any size of device, and is roughly one hundred times less than for self-sustained devices.

2. Discharge limiters altered the above figure by about 50%, probably due to field distortions.

3. The $CO:O_2$ ratio departed from 2:1 stoichiometry, as is typical of self-sustained devices, to a value of about 2.5:1.

4. CO does not attach and was found to have negligible effect on the discharge impedance.

5. The discharge impedance was found to rise linearly with oxygen partial pressure, doubling at 1% added oxygen. This arises from electron attachment.

6. The secondary current was found to depend linearly on the primary current, implying electron loss by attachment rather than recombination. $I_s:I_p$ was found to depend mainly on the ratio of readily ionised N_2 to electro-negative CO_2 in the gas mixture. For X:2:1 $He:N_2:CO_2$ mixtures $I_s:I_p$ was found to be about 3500.

7. Dissociation by the primary beam alone contributes about 10% of the total dissociation observed. It scales linearly with charge passed, the oxygen concentration rising at 15 millimoles/coulomb of primary current.

8. Like the main discharge effect, this rate did not change with volume, implying some kind of surface mediated phenomenon. The result should therefore be applicable to any size of laser.

9. Dissociation by primaries was measured as a function of CO_2 partial pressure to further investigate the process. The dependence was nonlinear, with an absorption isothermal shape suggesting a true dissociation process, perhaps akin to electron stimulated desorption.

10. The primaries appear to dissociate CO_2 with amazing efficiency, around 10%. 3000 CO_2 molecules are cracked by each primary electron. The process is not understood.

11. Gain measurements have been carried out on the P(20) line. Small signal gain was a sublinear function of E/N and main discharge current. Oxygen, produced by the discharge or deliberately added, influenced the gain only through changes in secondary current brought about by impedance alteration.

12. Dissociation has been shown to influence discharge stability only through impedance changes caused by oxygen formation.

TABLE 1

CATALYSTS FOR CO_2 LASERS

SECONDARY TO PRIMARY CURRENT RATIO

He : N_2 : CO_2	M
13 : 2 : 1	3500
3 : 2 : 1	3500
0 : 2 : 1	2500
3 : 2 : 0	6500
1 : 0 : 0	> 6000 (G → A)
0 : 1 : 0	4500
0 : 0 : 1	300

@ 4 kV cm^{-1} Atm^{-1}

$$M = \frac{\text{Secondary current}}{\text{Transmitted primary current}}$$

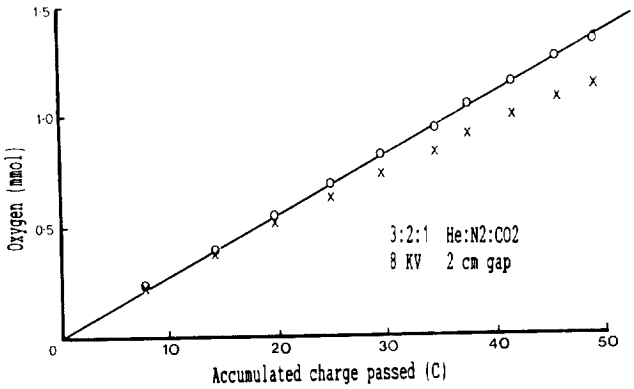

Fig. 5 Oxygen generation vs accumulated charge passed.

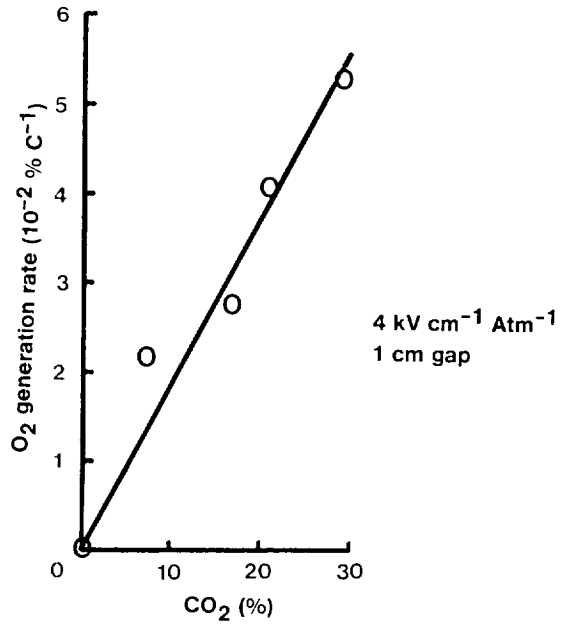

Fig. 6 Dependence of oxygen generation rate on carbon dioxide concentration.

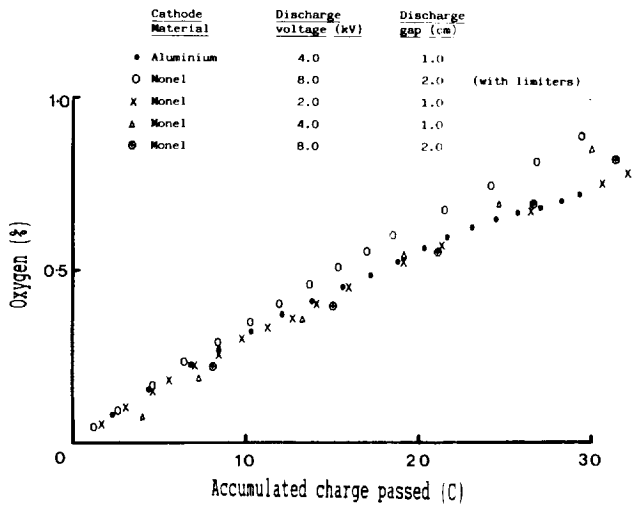

Fig. 7 Production of oxygen in discharge

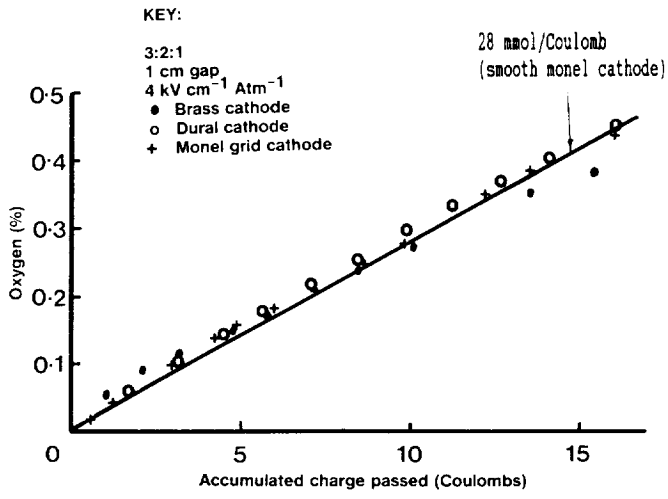

Fig. 8 Dependence of oxygen generation rate on cathode material and form.

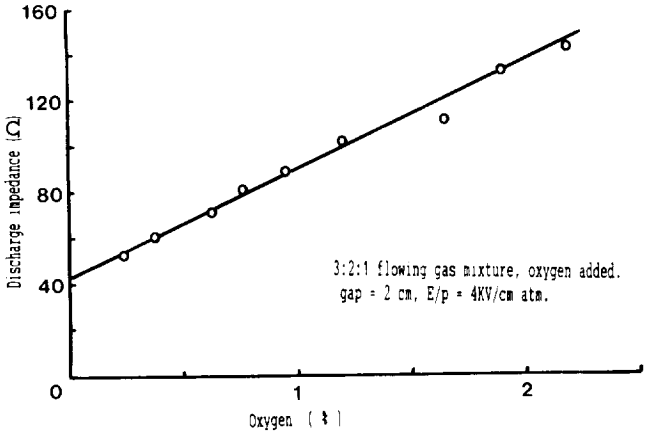

Fig. 13 Influence of oxygen on discharge impedance.

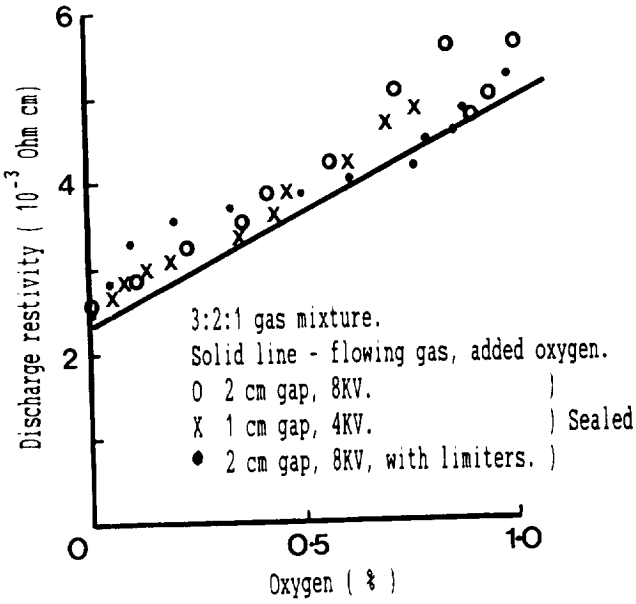

Fig. 14 Influence of oxygen on discharge restivity.

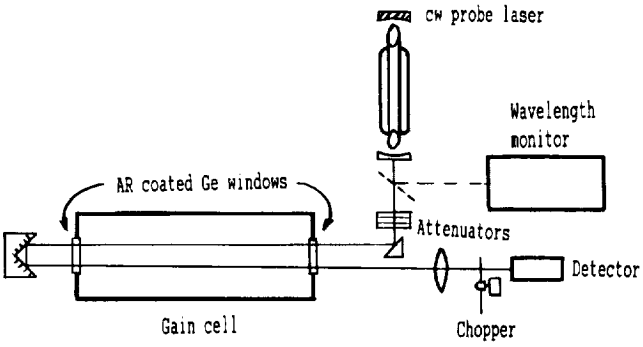

Fig. 15 Experimental arrangement for gain measurement.

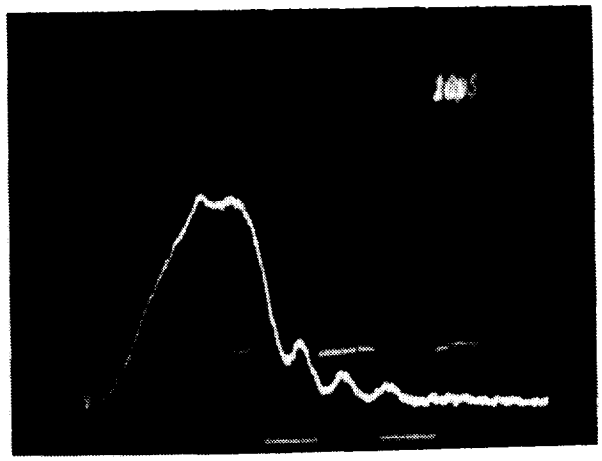

Fig. 16 Measurement of small signal gain.
Chopped signal 2mS/div
Gain signal 10 μS/div
3:2:1 He:N_2 :CO_2 + 1% O_2
10P(20)